Mechanism and kinetics of magnesium sulfite oxidation catalyzed by multiwalled carbon nanotube

Qiangwei Li, Yu Yang, Lidong Wang*, Peiyao Xu, Yinghui Han

School of Environmental Science and Engineering, North China Electric Power University, Baoding 071003, China

A B S T R A C T

Oxidation of magnesium sulfite is crucial for recycling the byproduct in magnesia desulfurization. Using impregnation method, a multiwalled carbon nanotube catalyst loaded with cobalt was prepared to promote the oxidation rate of magnesium sulfite ($MgSO_3$). The performance of catalysts impregnated by different concentration of $Co(NO_3)_2$ were compared, which showed that the optimal impregnating concentration was 30%. The catalysts prepared with various concentration of $Co(NO_3)_2$ were characterized by Brunauer–Emmett–Teller analysis, transmission electron microscopy, scanning electron microscopy, X-ray diffraction, and X-ray photoelectron spectroscopy. The catalyzed oxidation kinetics of magnesium sulfite was investigated in a bubbling tank, indicating that the general reaction orders with respect to carbon nanotube, oxygen, and magnesium sulfite were 0.22, 0.45, and 0.01, respectively. The apparent activation energy was 23.43 kJ mol^{-1}. The three-phases reaction model revealed that the internal diffusion of oxygen might be the rate-controlling step of magnesium sulphite oxidation. The results can serve as a useful reference for designing sulfite oxidation by using multiwalled carbon nanotube catalyst.

© 2016 Elsevier B.V. All rights reserved.

1. Introduction

Sulfur dioxide is a critical precursor to pollution such as acid rain and dust-haze. A magnesium oxide desulfurization technique is advantageous for its stable desulfurization efficiency, simple procedure, small land use, and low energy consumption [1,2]. Compared with limestone desulfurization, this technique is particularly applicable to treating fume produced through coal-fired industrial boilers in which the flow rate vary frequently; hence, it has been rapidly developed in recent years. However, this technique involves a slow oxidation reaction of $MgSO_3$, thus requiring additional costs and energy for recycling the byproducts of desulfurization. Moreover, incomplete oxidation of $MgSO_3$ easily induce problems including system structural blockage, low-quality products, and secondary pollution of sulfite. Therefore, in a magnesium desulfurization technique, facilitating the oxidation of $MgSO_3$ is a critical pathway for economically and effectively recycling desulfurization byproducts.

Regarding the catalytic reaction of $MgSO_3$ oxidation, scholars have mainly focused on the action of transition metal ions. Under industrial standards, Long [3] used $[Co(NH_3)_6]^{2+}/I^-$ to catalyze the

oxidation of $(NH_4)_2SO_3$ and confirmed that when the concentration of Co^{2+} is increased from 0.01 to 0.02 mol/L, the oxidation rate is increased by 2.85 times. Tatani [4] examined the crystallization and characteristics of $CaSO_3$ catalyzed by Mn^{2+}. The results verified that the degree of crystallinity of $CaSO_3$ increased linearly with the concentration of Mn^{2+} and that the crystallization ratio remained constant once the content of Mn^{2+} reached to approximately 10 mg/L. Karatza [5] used a laboratory-scale reaction device to investigate the actions of Cu^+ and Fe^{2+} ions in catalyzing the oxidation of $CaSO_3$ and reported that the catalytic effect of Fe^{2+} ions is greater than that of Cu^+ ions. Wang [6] adopted a bubbling apparatus to explore the catalytic effects of various transition metal ions on $MgSO_3$ and verified that Co^{2+} is the most effective catalyst facilitating the oxidation of $MgSO_3$. This finding agreed well with Zhu's report [2] that might be caused by the similar ion potential between transition metals with the cations in the sulfite [7], resulting in the replacement of Mg^{2+} by Co^{2+} which initiates the chain reaction. Overall, previous studies have indicated that Mn^{2+} and Co^{2+} exhibit the highest catalytic effect [8–12] and are thus prevalently investigated for their applications to $MgSO_3$ oxidation. Recent studies have mainly focused on the catalytic effects of transition metal ions. In practice, when a transition metal ion is used as a catalyst for desulfurization, the catalyst is continuously lost with the efflux of the desulfurization solution. In addition, the catalyst can enter the oxidation product, thus expending excessive

---

Nomenclature

c_b	Reactant concentration in the solution phase, mol/L
c_{Co}	Concentration of cobalt in the liquid bulk, mol/L
c_i	Reactant concentration above the interface, mol/L
c_{O_2}	Concentration of oxygen in the liquid bulk, mol/L
$c_{S(IV)}$	Concentration of sulfite in the liquid bulk, mol/L
D_{ed}	Mass diffusion coefficient on catalyst external surface, m^2/s
D_{int}	Mass diffusion coefficient on catalyst internal surface, m^2/s
$k_1 \sim k_5$	Rate constant from Eq. (1)–(5) respectively
k_{in}	Coefficient of intrinsic reaction rate, L/(mol s)
L	Pore length of the CNTs catalyst, m
mL	Thiele module
n	Reaction order of oxygen in the intrinsic reaction
p	Reaction order of sulfite in the intrinsic reaction
q	Reaction order of cobalt in the intrinsic reaction
r_{ed}	External diffusion rate, mol/(L s)
r_{id}	Internal diffusion rate, mol/(L s)
r_{in}	Intrinsic reaction rate, mol/(L s)

costs and incurring secondary pollutants. Therefore, developing recyclable solid catalysts becomes an essential topic concerning desulfurization techniques. In our previous research on the catalytic kinetics of metal ions [6], Co^{2+} were loaded onto the surface of a molecular sieve to accelerate the oxidation of SO_3^{2-}. The results of this research were favorable, indicating that the oxidation rate was increased by 25% to 190% with the addition of molecular sieve ranging from 10 to 80 mg L^{-1}.

In recent years, the preparation methods of catalysts supported on inorganic carriers have received the attention of various scholars [13–16]. Applying carbon nanotubes (CNTs), a novel inorganic carbon-structure material discovered by Iijima [17] in 1991, as catalyst carriers have received the recognition of scholars. This type of material is advantageous for its acid and alkali resistance, high toughness [18], large hollow structure, and high surface area. Currently, integrating a catalyst and CNTs mainly involves the immersion method [19–21]. Because the surface of a CNTs is hydrophobic [22,23], the aqueous solvents used in the immersion method cannot be applied; instead, organic solvents such as ethanol [22], benzene [23], and acetone [24] are used as the active ingredient solvent. Nhut et al. loaded Pd onto the surface of CNTs [25] to catalyze the hydrogenation of cinnamaldehyde and confirmed that the activity of the catalyst was favorable, with a selective of approximately 80%. Xu et al. adopted an arc discharge method to load Ni onto CNTs [26], which were then applied to the hydrodesulfurization of gasoline and diesel. Their results revealed that the catalyst was highly functional; specifically, the Ni-CNTs catalyst facilitated decreasing the sulfur content from 1126 mg/L to 10 mg/L after 4 h of hydrodesulfurization. Yang et al. loaded Pd/PdO and Pd onto multiwalled CNTs [27] (MWCNTs) and applied them to water treatment; the results revealed that the catalytic effect of the compound activity factor Pd/PdO-MWCNTs is higher than that of single activity factor Pd-MWCNTs. Li et al. loaded dissimilar ratios of Co-Mo (0.2, 0.35, 0.5, and 0.7) into CNTs [28] using the immersion method to conduct the hydrodesulfurization of diesel fuel and gasoline. Their results showed that the desulfurization efficiency of the Co-Mo/CNTs catalyst was 54.08%. Nevertheless, little research have investigated applying the CNTs loading technique to conducting wet desulfurization and preparing solid catalysts.

This study mainly focused on the oxidation of $MgSO_3$ by adopting CNTs as a carrier to prepare a Co-based catalyst. In addition, a research method investigating kinetic mechanisms was used to explore the oxidation reaction mechanism of $MgSO_3$ under the presence of CNTs catalyst. The results of this study can serve as a reference for developing a technique to enable recycling the desulfurization byproduct by sulfite oxidation.

2. Experimental

2.1. Preparation of the CNTs catalyst

Two grams of CNTs were placed in an Erlenmeyer flask, followed by 150 mL of 60% NHO_3. The mixture was heated (80 °C), stirred, and condensed using a reflux condenser for 5 h. The product was then vacuum filtered and washed until pH = 7, followed by drying at 120 °C for 2 h. Next, the product was immersed in $Co(NO_3) \cdot 6H_2O$ solutions of dissimilar concentrations (10%, 20%, 30%, and 40%), and 50 mL anhydrous ethanol was added to each solution, which was stirred at 30 °C and then dispersed using an ultrasonic dispersion equipment for 30 min. The products were dried for 2 h at 120 °C and then roasted in a tube furnace fluxed with N_2. The roasting temperature was configured as follows: The temperature was raised to 120 °C over a period of 1 h and then maintained at 120 °C for 1 h. Next, the temperature was raised to 500 °C over a period of 2 h and then maintained at 500 °C for 3 h.

2.2. CNTs catalyst characterization

The Brunauer, Emmett, and Teller (BET) method was used to determine the specific surface area, adsorption capacity, and carbon content of the catalyst (SA31000). The internal morphology, phase characteristics, and crystal grain size of the catalyst were examined using transmission electron microscopy (TEM; JEM-2100), and the surface and cross-section morphological features of the catalyst were investigated using scanning electron microscopy (SEM; S4800). An X-ray microanalysis system (System 7, EDS) was employed to conduct quantitative analysis on the elemental distribution in the microscopic regions of the catalyst. X-ray diffraction (XRD; Bruker D8 Advance) was used to conduct qualitative and quantitative analyses on the crystalline substance of the catalyst. X-ray photoelectron spectroscopy (XPS; ESCALAB 250) was applied to analyze the surface elemental composition and valence of the catalyst.

2.3. Kinetics of magnesium sulfite oxidation catalyzed by CNTs

The magnesium sulfite sample as a mixture of hydrated sulfite was prepared by vacuum evaporation method [29] and detected by TG analysis. The content of $MgSO_3 \cdot 3H_2O$ in this hydrate sulfite mixture is calculated to be about 29.7%, and $MgSO_3 \cdot 6H_2O$ is 70.3%. A bubbling tank reactor was employed to investigate the oxidation kinetics of magnesium sulfite (Fig. 1). After supplying 200 mL of deionized water, the CNTs catalyst was added into the reactor. Pure oxygen, nitrogen, and compressed air were blended and injected in the reactor as the oxidation gas. The reaction was then initiated by adding magnesium sulfite into the reactor. The hydrochloric acid and sodium hydroxide solution was used for pH adjustment. It is noted that the hydrochloric acid was added into the well mixed slurry drop by drop to avoid the effusion of SO_2 during the pH adjustment. A trace amount of the reaction solution was pipetted at regular intervals, dissolved in hydrochloric acid, and diluted for measurement. The sulfate concentration at various time points t was determined using barium sulphate spectrophotometry. The results showed that the sulfate concentration increased linearly with increasing reaction time, in which the slope k denotes the oxidation rate of the magnesium sulfite.
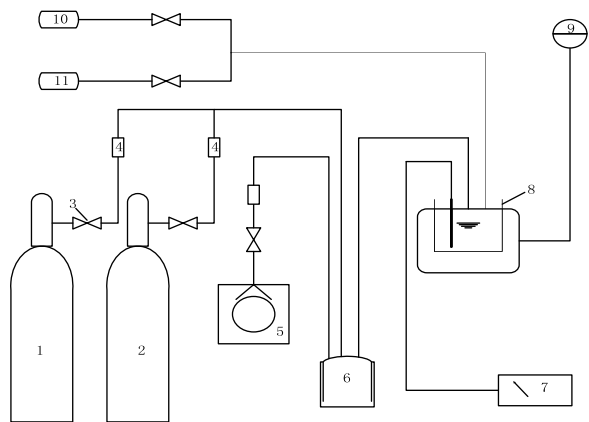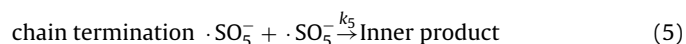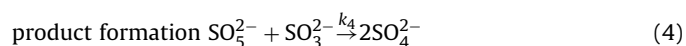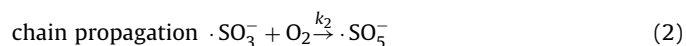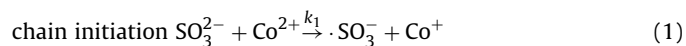
Fig. 1. Apparatus of catalyzed oxidation of magnesium sulfite.

1-pure nitrogen, 2-pure oxygen, 3- decompression valve, 4- LZB-4 glass rotameter, 5- TYW-1 air compressor, 6- buffering bottle, 7- PHS-3C pH meter, 8-glass reactor in volume of 500 mL, 9-85-2A magnetism heating mixer, 10-hydrochloric acid solution in concentration of 3 mol L^{-1}, 11-sodium hydroxide solution in concentration of 1 mol L^{-1}.

3. Experimental results

3.1. Catalyst activity assessment

The homogeneous oxidation of sulfite catalyzed by Co^{2+} was reported [12,29] as a chain reaction

$$\text{chain initiation } SO_3^{2-} + Co^{2+} \overset{k_1}{\rightarrow} \cdot SO_3^- + Co^+ \tag{1}$$

$$\text{chain propagation } \cdot SO_3^- + O_2 \overset{k_2}{\rightarrow} \cdot SO_5^- \tag{2}$$

$$\cdot SO_5^- + SO_3^{2-} \overset{k_3}{\rightarrow} SO_5^{2-} + \cdot SO_3^- \tag{3}$$

$$\text{product formation } SO_5^{2-} + SO_3^{2-} \overset{k_4}{\rightarrow} 2SO_4^{2-} \tag{4}$$

$$\text{chain termination } \cdot SO_5^- + \cdot SO_5^- \overset{k_5}{\rightarrow} \text{Inner product} \tag{5}$$

According to the experimental setup depicted in Fig. 1 for the aforementioned devices, the initial amount of MgSO$_3$ was 10.0 g, the CNTs concentration was 1.5 g/L, the air flow rate was 60 L/h, the oxygen vapor pressure was 0.21 atm, the temperature was 45 °C, the stirring rate was 860 r/min, the total volume of the reaction solution was 200 mL, and the pH was 8. As the immersion concentration of Co^{2+} increased, the Co content on the surface of CNTs gradually increased. Fig. 2 illustrates the effect of Co concentration on the oxidation rate of MgSO$_3$.

Co^{2+} has been proven the most efficient catalyst for promoting the oxidation rate of magnesium sulfite [29] by initiating the chain reaction [30,31]. As shown in Fig. 2, the uncatalyzed reaction rate, approximately 0.0086 mmol/(L·s), was close to that with the pure CNTs carrier, indicating CNTs is not the active phase. In contrast, the reaction rate was found substantially facilitate with the increase of Co loading, showing that Co is the active phase. When the immersion concentration reached 30%, the oxidation rate of MgSO$_3$ peaked at approximately 0.0694 mmol/(L s), which was 5.45 times higher than that under the noncatalytic condition. However the catalysis performance was also affected by the distribution of Co on the CNTs carrier. When the Co loading increased higher than 30%, the active Co particles might aggregate and overlap on the carrier which caused the catalysis performance decline.

Moreover, at the ending of each experiment, the Co^{2+} concentration dissolving from the CNTs catalyst was measured by atomic absorption spectrometry. It was found that the Co^{2+} is undetected due to its low amounts, indicating that the binding of Co with the CNT carrier is firm enough to ensure the lifespan of catalyst. Moreover, the high operating pH (at 8.0) also might prohibit the dissolution of Co from the catalyst.

3.2. Catalyst characterization

3.2.1. N$_2$ adsorption–desorption isotherms of CNTs catalyst

The BET method involved examining the nitrogen adsorption–desorption isotherms of the samples. Each sample was dried at 393 K for 12 h. Fig. 3 illustrates the adsorption–desorption isotherm and pore distribution of the catalyst. The results revealed that the adsorption–desorption isotherm of the catalyst was categorized as a Type IV isotherm featuring a Type H3 hysteresis loop, indicating that the catalyst pertains to a mesoporous material with even pore size. A Type IV isotherm exhibits low adsorption at low pressure, and the adsorption increases with pressure; accordingly, the pores the catalyst were filled. The specific surface areas of the CNTs samples obtained through the immersion concentrations of 10%, 20%, 30%, and 40% were 97.37, 96.74, 74.89, and 63.81 m^2/g, respectively, which was in good agreement with Fu's results [32].

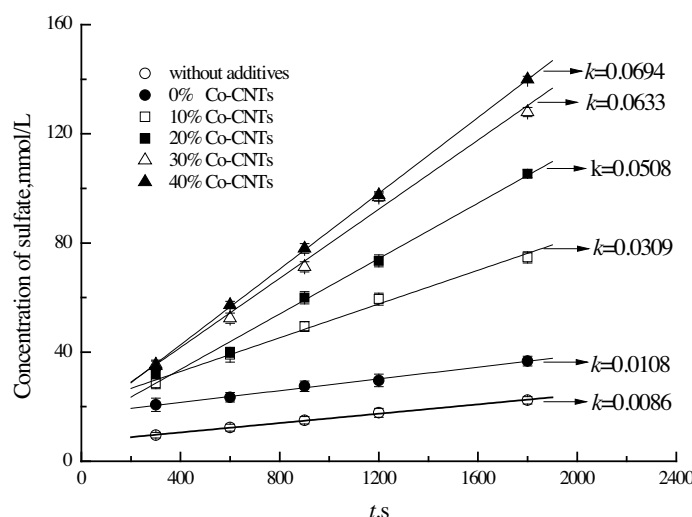**Fig. 2.** Comparison of catalytic performance of CNTs impregnated with different levels of Co loading.
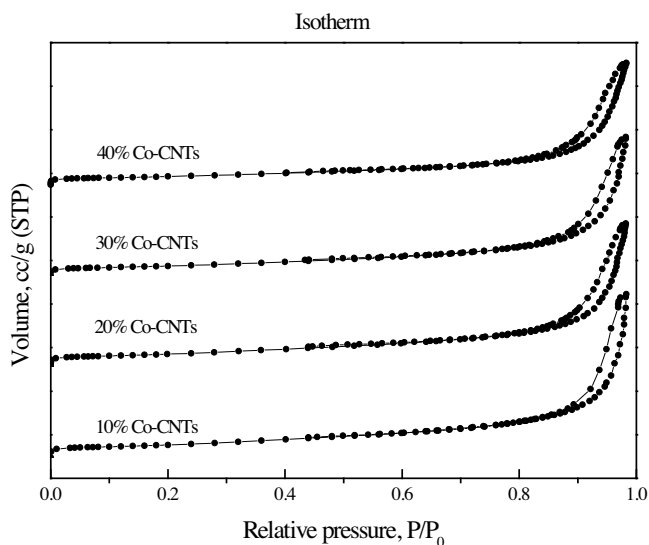
Isotherm

Fig. 3. Comparison of N_2 Adsorption–desorption Isotherms of CNTs impregnated with different levels of Co loading.

The adsorption capacities were found to be 22.38, 22.73, 17.22, and 14.47 cm^3/g, respectively. This indicates that as the loading of Co increases, the pores of the CNTs are filled with additional substances; hence, the specific surface area and adsorption capacity of the catalyst decreased. However, examining the results of Fig. 2 revealed that the changes in the pore size and specific surface area did not exert a substantial effect on the activity of the catalyst.

3.2.2. TEM patterns of CNTs catalyst

Fig. 4 illustrates the microscopic structure (e.g., internal morphology as well as crystal structure, size, and defect) of CNTs [24,25]. The TEM conditions were configured as follows: accelerating voltage = 20–200 KV; dot resolution = 0.235 nm; lattice resolution = 0.14 nm; magnifying ratio = 250,000 to 1,000,000×; and X-ray energy-dispersive resolution = 127 eV (Be-U). Figs. 4(a)–(d) depict the TEM images (0.2 μm and 200 nm high-resolution TEM) of CNTs obtained under various Co immersion concentrations.

The results showed that the loading volumes in Fig. 4(a) and (b) were notably less than those in Fig. 4(c) and (d). However, the loading volume displayed in Fig. 4(d) was notably high, inducing the aggregation of Co, thereby blocking some of the active sites. This result accords with that of Fig. 2, verifying that when the immersion concentration of Co was increased from 30% to 40%, the catalytic rate was reduced.

3.2.3. SEM patterns of CNTs catalyst

The CNTs catalyst was dispersed in ethanol using an ultrasonic device for 30 min. A disposable pipette was used to load one drop of the catalyst onto the back of an aluminum foil. An ear syringe was used to blow away the ethanol solvent. The location of the catalyst droplet was marked using a marker pen. After the droplet dried, the aluminum foil was placed on the sample platform to capture its SEM image. Fig. 5 illustrates the SEM images the CNTs catalysts prepared using various Co immersion concentrations. Particularly, a trace amount of Co particles is observed in Fig. 5(a), whereas the amount of Co particles in Fig. 5(b) is slightly higher. The amount of Co particles in Fig. 5(c) notably increases. Finally, Co particle aggregation is observed in Fig. 5(d), in which small and dispersed particles aggregate to form large particles. The SEM results further verified the results of Figs. 2 and 4.
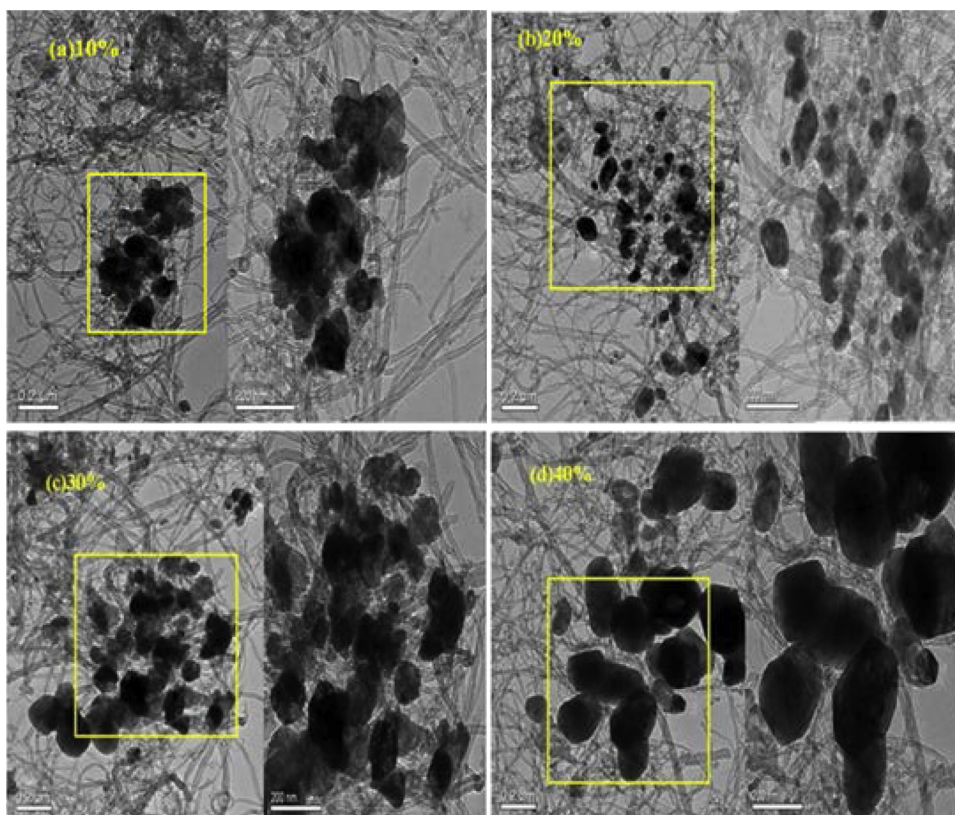

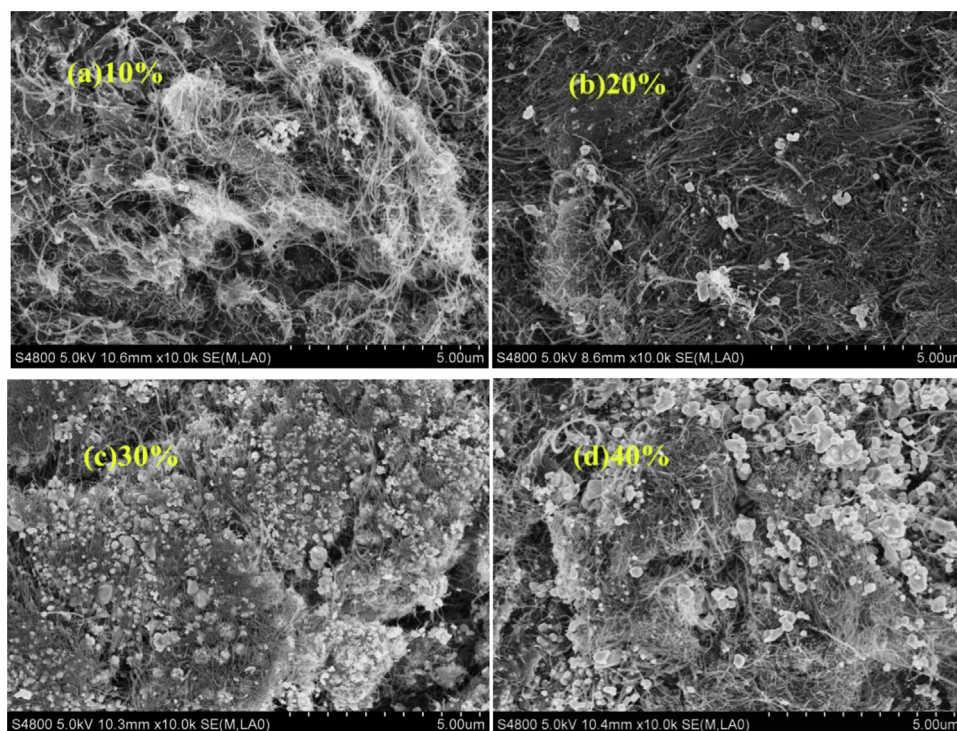**Fig. 4.** Comparison of TEM patterns of CNTs impregnated with different levels of Co loading.

Fig. 5. Comparison of SEM patterns of CNTs impregnated with different levels of Co loading.
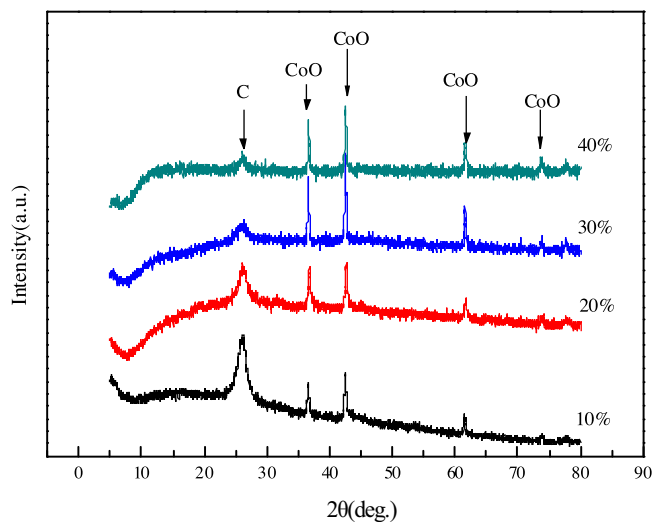

Fig. 6. Comparison of XRD patterns of CNTs impregnated with different levels of Co loading.

3.2.4. XRD patterns of CNTs catalyst

Fig. 6 depicts the XRD spectra of CNTs catalysts prepared using dissimilar Co loading volumes. The XRD scan angle ranged between $5°$ and $80°$, and the scan rate was set as $0.1°$/min. The diffraction peak at 26^0 (002) corresponds to the carbon nanotube [33]. It was observed that the intensity of this peak gradually decreased with an increase in cobalt loading, which is believed to be attributable to the incorporation of cobalt atoms within the graphene lattice [34,35]. This observation also agrees with the results reported in other researches of Co/CNTs catalysts [36,37].

When the Co loading volume increased from 10% to 30%, the diffraction peaks of CoO at $36.3°$, $42.5°$, $61.7°$, and $73.8°$ gradually increased. When the Co loading volume reached 30%, the strongest diffraction peak was observed at $42.5°$. By contrast, when the Co

loading volume reached 40%, the diffraction peaks of C and CoO were weaker than those observed when the Co loading volume was 30%. This might be attributable to how Co cannot be adsorbed to the surface of CNTs when the content of Co is excessively high, reducing the activity of the catalyst, thereby weakening the corresponding diffraction peaks [38]. This finding accords with those of Figs. 2, 4 and 5.

3.2.5. XPS patterns of CNTs catalyst

XPS was employed to further analyze the composition and valence of the CNTs samples prepared using dissimilar Co immersion concentrations. Fig. 7 illustrates the spectra of C1s graphite, O1s, CoNtv Ox, and Co_3O_4. Adjusting the binding energy peaks revealed that the main peaks of C1s (Fig. 7(a)) and O1s (Fig. 7(b)) appeared at 285.0 and 532.0 eV, respectively. When the Co content was increased from 10% to 40%, the peak area of O1s gradually increased, indicating that Co might exist in the oxidized form. Adjusting the binding peaks of CoNtv Ox and Co_3O_4 (Fig. 7(c)) showed that the main peaks appeared at 780.9 and 779.5 eV, respectively. The peak area of CoNtv Ox was the greatest when the Co content was 30%, indicating that under this Co content ratio, the amount of active Co in the catalyst was the greatest. This finding further verified those of the XRD analysis, which revealed that when the Co content was 30%, the strongest peak was observed at $42.5°$.

3.3. Kinetics of magnesium sulfite oxidation

The following experiments were conducted using the Co-CNTs catalyst which was prepared with the cobalt immersion concentrations of 30%. As shown in Fig. 8, increasing the concentration of the catalyst accelerated the reaction rate of $MgSO_3$ oxidation, indicating that the catalyst exerted a noticeable effect on facilitating the oxidation of $MgSO_3$. When the concentration of the catalyst ranged between 0.5 and 3.0 g/L, the reaction rate of $MgSO_3$ oxidation was increased by 3.2 to 5.3 times, respectively. The catalyst concen-
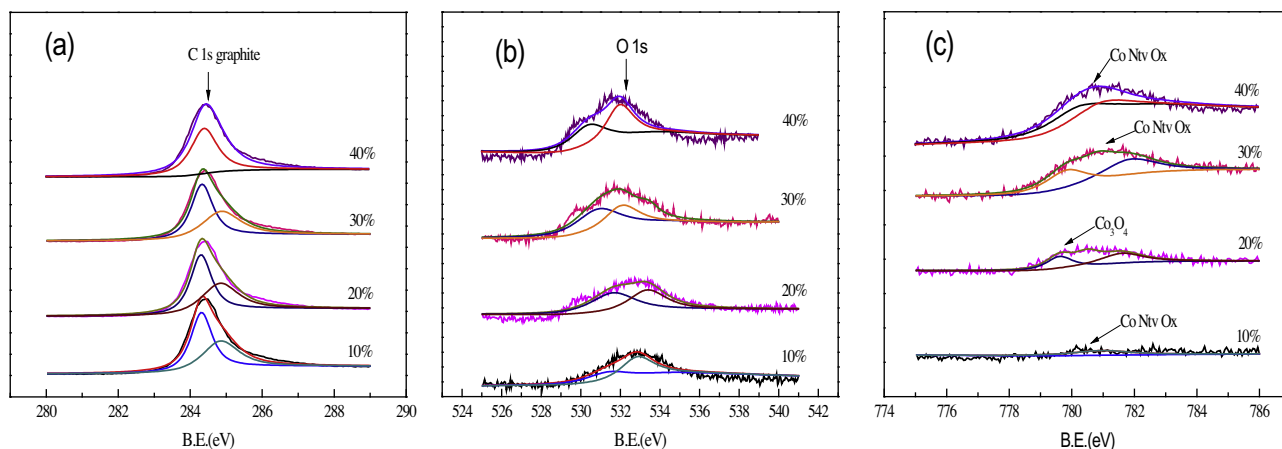
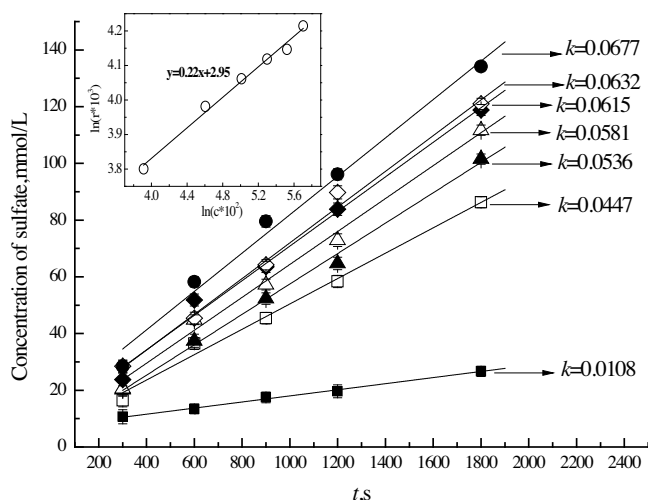**Fig. 7.** Comparison of XPS patterns of CNTs impregnated with different cobalt loading.

Fig. 8. Effect of Co-CNTs concentration on the oxidation rate: ■ 0 g/L; □ 0.5 g/L; ▲ 1.0 g/L; △ 1.5 g/L; ◆ 2.0 g/L; ◇ 2.5 g/L; ● 3.0 g/L $c_{S(IV)}$ = 50 g/L, P_{O_2} = 0.21 atm, Q = 60 L/h, T = 318 K and pH = 8.0.
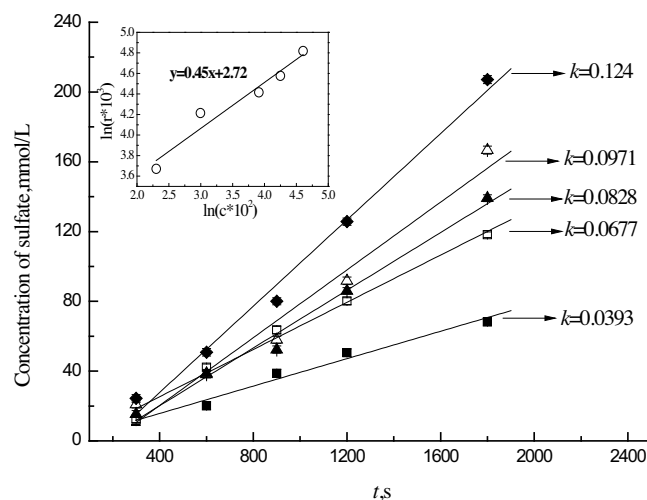

Fig. 9. Effect of oxygen partial pressure on the oxidation rate: ■ 0.10 atm; □ 0.20 atm; ▲ 0.50 atm; △ 0.70 atm; ◆ 1.00 atm $c_{S(IV)}$ = 50 g/L, c_{CNTs} = 3.0 g/L, Q = 60 L/h, T = 318 K, and pH = 8.0.

tration and reaction rate values were converted to dimensionless values, and then logarithmic operations were employed to calculate the rate order of the catalyst, which was approximately 0.22. Compared with the aqueous Co^{2+} catalysis with the reaction order of 0.5 [29], the overall reaction rate in the current work, probably being controlled by the mass transfer of oxygen instead of intrinsic reaction, was less sensible in the supported CNTs catalyst loaded with CoOx.

Fig. 9 illustrates that the reaction rate of $MgSO_3$ oxidation increases with increasing oxygen partial pressure. According to the Henry's law, oxygen partial pressure pertains to the equilibrium concentration of dissolved oxygen at the gas–liquid interface. Therefore, in the oxidation of $MgSO_3$, increasing the oxygen partial pressure increased the equilibrium concentration of oxygen at the gas–liquid interface; accordingly, the reaction rate of $MgSO_3$ oxidation increased. The oxygen partial pressure and oxidation rate values were converted to dimensionless values. Next, logarithmic operations were used to determine the linear correlation between the two values. The slope of the linear correlation line was equal to the rate order of the oxygen partial pressure (0.45). This finding agreed well with Wang's reports [39], in which the cobalt was loaded on the molecular sieve carrier in order to expedite the sulfite oxidation.
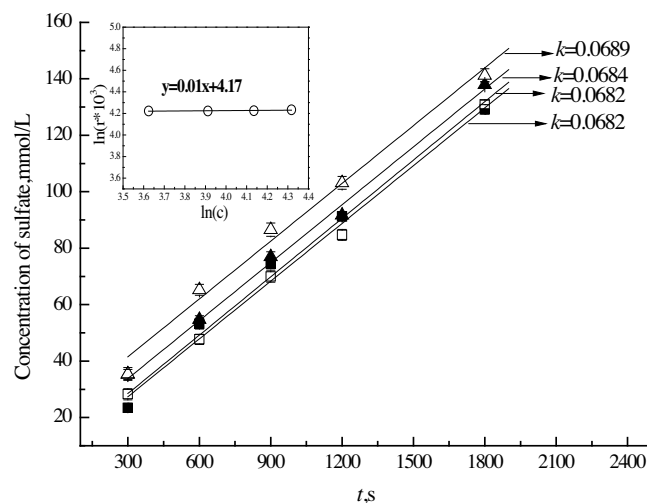

Fig. 10. Effect of magnesium sulfite concentration on the oxidation rate: ■ 37.5 g/L; □ 50.0 g/L; ▲ 62.5 g/L; △ 75.0 g/L c_{CNTs} = 3.0 g/L, P_{O_2} = 0.21 atm, Q = 60 L/h, T = 318 K, and pH = 8.0.
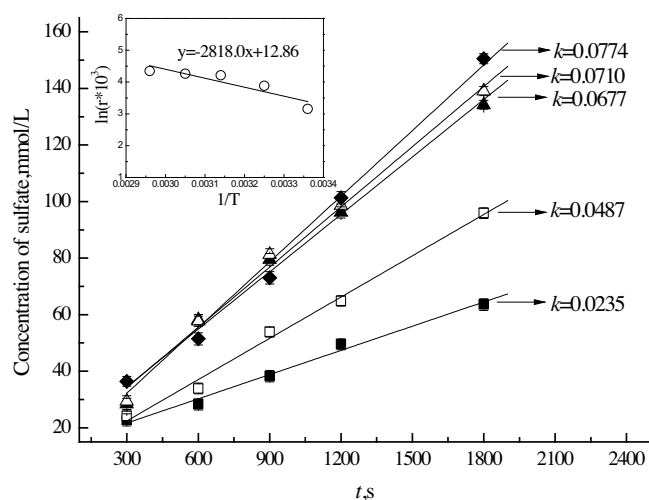
Fig. 11. Effect of temperature on the oxidation rate: ■ 298 K; □ 308 K; ▲ 318 K; △ 328 K; ◆ 338 K $c_{S(IV)}$ = 50 g/L, c_{CNTs} = 3.0 g/L, P_{O_2} = 0.21 atm, Q = 60L/h, and pH = 8.0.

As shown in Fig. 10, the initial concentration of MgSO₃ exerted a minor effect on the reaction rate of MgSO₃ oxidation. In other words, MgSO₃ oxidation is a zero order reaction with respect to the concentration of MgSO₃. This is attributable to the low solubility of MgSO₃, approximately 0.87 g at 45 °C [40], which is much lower than Na₂SO₃ and (NH₄)₂SO₃. Under the experimental conditions of the present study, the concentration of MgSO₃ was oversaturated; hence, increasing the MgSO₃ concentration did not increase the amount of dissolved MgSO₃. Accordingly, the rate of MgSO₃ oxidation did not exhibit notable changes. The catalyst concentration and reaction rate values were converted to dimensionless values. Next, logarithmic operations were employed to determine the rate order of MgSO₃ (0.01). This observation agreed well with Wang [39] and Long [3], which might be caused by the saturation of sulfite, resulting the independency of overall reaction rate on the initial sulfite concentration.

As depicted in Fig. 11, the reaction rate of MgSO₃ oxidation increased with increasing reaction temperature. The logarithm of the reaction rate was adopted to plot a 1/T diagram, the linear line slope of which was 2818.0. The results showed that when the reaction temperature was between 298 and 338 K, and the effect of temperature to reaction rate accorded with the Arrhenius law. Accordingly, the activation energy (Ea) of MgSO₃ was determined as 23.43KJ/mol. Compared with our published result of molecular sieve catalyst [39], the immersion concentrations of cobalt approached to 30%, which might considerably enrich the active sites and lower the activation energy.

4. Discussion

The oxidation of MgSO₃ pertains to a complex multiphase reaction that mainly involves intrinsic reaction rate, external surface diffusion, and internal surface diffusion [39]. In the present study, the intrinsic reaction involved the desorption of the reactants and oxidation products; external surface diffusion was the process through which MgSO₃ and oxygen (reactants) diffused from the solution-phase to the surface of the solid-phase catalyst; internal surface diffusion pertained to how MgSO₃ entered the internal surface of the catalyst and underwent the oxidation process within the catalyst.

4.1. Intrinsic reaction rate

According to Barron et al. [41,42], the intrinsic reaction rate of Co-catalyzed SO₃²⁻ is described as (6):

$$r_{in} = k_{in}c_{O_2}{}^n c_{S(IV)}{}^p c_{Co}{}^q \qquad (6)$$

where n = 0, p = 1.5, and q = 0.5.

As shown in Figs. 8–10, the reaction orders of the CNTs catalyst, oxygen partial pressure, and MgSO₃ were 0.23, 0.45, and 0.01, respectively. These values differ from those of (6). Moreover, under intrinsic reaction conditions, temperature exerts a notable effect on reaction rate, and the apparent activation energy is usually greater than 50 KJ/mol; this contradicts with the results of Fig. 11. Therefore, we infer that the overall catalyzed oxidation reaction of MgSO₃ investigated in this study is not affected by intrinsic reaction processes.

4.2. Diffusion rate on catalyst external surface

The rate of which a reactant diffuses to the surface of a catalyst is calculated as follows:

$$r_{ed} = D_{ed}(c_b - c_i) \qquad (7)$$

Omitting c_i yields:

$$r_{ed} \approx D_{ed}c_b \qquad (8)$$

Equation (7) indicates that when the overall reaction is controlled by the external diffusion process, the overall reaction rate is directly correlated to the reactant concentration in the solution phase; this contradicts with the results of Fig. 9. Furthermore, under this condition, the overall reaction rate is insensitive to temperature variations, and the activation energy is generally between 4.2 and 21 KJ/mol. Fig. 11 displays that the activation energy of MgSO₃ oxidation is 23.4 KJ/mol, which does not meet the basic condition of external diffusion effect. Therefore, when the proposed catalyst is used, the oxidation of MgSO₃ is not affected by the diffusion of the reactants on the surface of the catalyst.

4.3. Diffusion rate on catalyst internal surface

The diffusion rate of a reactant in the pores of a catalyst can be described [43] using the Thiele model (9):

$$mL = L\sqrt{k_{in}/D_{int}} \qquad (9)$$

Under irreversible n-order reaction conditions, mL is defined as follows:

$$mL = L\left[(n+1)k_{in}c_A{}^{n-1}/(2D_{id})\right]^{1/2} \qquad (10)$$

According to the experimental results of an intrinsic reaction, the diffusion rate of MgSO₃ within the proposed catalyst can be calculated using (11):

$$r_{id} = \left[2k_{in}D_{id}/(n+1)L^2\right]^{1/2} c_{O_2}{}^{(n+1)/2} c_{S(IV)}{}^{p/2} c_{Co}{}^{q/2} \qquad (11)$$

The reaction rate can be calculated using (12):

$$r_{id} = k_{in}c_A{}^n (1/mL) = k_{in}c_A{}^n (1/L)\left[2D_{id}/(n+1)k_{in}c_A{}^{n-1}\right]^{1/2}$$
$$= \left[2k_{in}D_{id}/(n+1)L^2\right]^{1/2} c_A{}^{(n+1)/2} \qquad (12)$$

Equation (12) indicates that under the internal diffusion condition, the overall reaction rate is positive correlated to the (n + 1)/2th power of oxygen concentration and to the q/2th power of Co concentration. This accords with the experimental results of Figs. 8 and 9. Under the experimental conditions of the present study, the concentration of MgSO₃ was oversaturated; hence, the

overall reaction rate was not affected by the concentration of MgSO$_3$. Moreover, under the internal diffusion effect, the sensitivity of the overall reaction rate toward temperature is higher than that under the external diffusion effect, and the activation energy is generally between 21 and 50 KJ/mol. According to the aforementioned assertions, under the experimental conditions of the present study, the reaction rate of MgSO$_3$ oxidation was controlled by the reactant diffusion mechanism on the internal surface of the catalyst.

Acknowledgement

References

[1] Z. Shen, S. Guo, W. Kang, K. Zeng, M. Yin, J. Tian, J. Lu, Fuel 105 (2013) 578–584.
[2] T. Zhu, Y. Ma, H. Zhang, D. Li, L. Li, X. Zhou, B. Song, J. Hao, Catal. Today 258 (2015) 70–74.
[3] X. Long, W. Li, W. Xiao, W. Yuan, J. Hazard. Mater. 129 (2006) 260–265.
[4] A. Tatani, T. Imai, Y. Fujima, J. Chem. Eng. Jpn. 36 (2003) 1057–1062.
[5] D. Karatza, M. Prisciandaro, A. Lancia, D. Musmarra, Chem. Eng. J. 145 (2008) 285–289.
[6] L. Wang, J. Wang, P. Xu, Q. Li, W. Zhang, S. Cui, S. Liu, Appl. Catal. A-Gen. 511 (2016) 16–22.
[7] A. Kiejna, Chemnitz 131 (1991) 117–121.
[8] A. Lancia, D. Musmarra, M. Prisciandaro, M. Tammaro, Chem. Eng. Sci. 54 (1999) 3019–3026.
[9] B. Zhao, Y. Li, H. Tong, Y. Zhuo, L. Zhang, J. Shi, C. Chen, Chem. Eng. Sci. 60 (2005) 863–868.
[10] A.A. Shaikh, S.M.J. Zaidi, React. Kinet. Catal. Lett. 64 (1998) 343–349.
[11] A. Lancia, D. Musmarra, F. Pepe, M. Prisciandaro, Chem. Eng. J. 66 (1997) 123–129.
[12] V. Linek, V. Vacek, Chem. Eng. Sci. 36 (1981) 1747–1768.
[13] L. Wang, R. Yang, C. Sun, AIChE J. 59 (2013) 29–32.
[14] H. Farag, Appl. Catal. B-Environ. 84 (2008) 1–8.
[15] K. Yan, T. Lafleur, J. Liao, J. Nanopart. Res. 15 (2013) 1–7.
[16] T. Onoe, S. Iwamoto, M. Inoue, Catal. Commun. 8 (2007) 701–706.
[17] S. Iijima, National 354 (1991) 56–58.
[18] Z. Wang, P. Poncharal, W.A. de Heer, J. Phys. Chem. Solids 61 (2000) 1025–1030.
[19] A.I. Dugulan, J.A.R. van Veen, E.J.M. Hensen, Appl. Catal. B-Environ. 142–143 (2013) 178–186.
[20] H. Shang, C. Liu, Y. Xu, J. Qiu, F. Wei, Fuel Process. Technol. 88 (2007) 117–123.
[21] H. Zhang, C. Sun, F. Li, H. Li, H. Cheng, J. Phys. Chem. B 110 (2006) 9477–9481.
[22] N.M. Rodriguez, M.S. Kim, R.T.K. Baker, J. Phys. Chem. 98 (1994) 13108–13111.
[23] Y. Zhang, H. Zhang, G. Lin, P. Chen, Y. Yuan, K.R. Tsai, Appl. Catal. A-Gen. 187 (1999) 213–224.
[24] H. Chen, J. Lin, Y. Cai, X. Wang, J. Yi, J. Wang, G. Wei, Y. Lin, D. Liao, Appl. Surf. Sci. 180 (2001) 328–335.
[25] J.M. Nhut, R. Vieira, L. Pesant, J.P. Tessonnier, N. Keller, G. Ehret, C. Pham-Huu, M.J. Ledoux, Catal. Today 76 (2002) 11–32.
[26] K. Xu, Y. Li, X. Xu, C. Zhou, Z. Liu, F. Yang, L. Zhang, G. Wang, J. Gao, C. Xu, Fuel 160 (2015) 291–296.
[27] F. Yang, C. Chi, S. Dong, C. Wang, X. Jia, L. Ren, Y. Zhang, L. Zhang, Y. Li, Catal. Today 256 (2015) 186–192.
[28] C. Li, B. Shi, M. Cui, H. Shang, G. Que, J. Fuel Chem. Technol. 35 (2007) 407–411.
[29] Q. Li, L. Wang, Y. Zhao, Y. Ma, S. Cui, S. Liu, P. Xu, J. Hao, Environ. Sci. Technol. 48 (2014) 4145–4152.
[30] B. Sun, P. Li, Y. Liang, M. Arowo, J. Wang, H. Meng, J. Chen, L. Shao, Chem. Eng. J. 253 (2014) 258–263.
[31] P.K. Das, S. Anand, R.P. Das, Scand. J. Metall. 24 (1995) 152–158.
[32] T. Fu, R. Liu, J. Lv, Z. Li, Fuel Process. Technol. 122 (2014) 49–57.
[33] U. Ritter, P. Scharff, G.E. Grechnev, V.A. Desnenko, A.V. Fedorchenko, Carbon 49 (2011) 4443–4448.
[34] T. Fu, Z. Li, Catal. Commun. 47 (2014) 54–57.
[35] T. Battumur, S.B. Ambade, R.B. Ambade, P. Pokharel, D.S. Lee, S. Han, W. Lee, S.H. Lee, Curr. Appl. Phys. 13 (2013) 196–204.
[36] S. Karimi, A. Tavasoli, Y. Mortazavi, A. Karimi, Appl. Catal. A 499 (2015) 188–196.
[37] M. Tre′panier, A. Tavasoli, A.K. Dalai, N. Abatzoglou, Appl. Catal. A 353 (2009) 193–202.
[38] B. Li, X. Jin, Y. Zhu, Inorg. Chim. Acta 419 (2014) 66–72.
[39] L. Wang, S. Cui, Q. Li, J. Wang, S. Liu, Appl. Catal. A 511 (2016) 16–22.
[40] X. Cao, X. Chen, Nonferrous Met. Eng. Res. 21 (2000) 47–51.
[41] C.H. Barron, H.A. O'Hern, Chem. Eng. Sci. 21 (1966) 397–404.
[42] W. Pasluk-Bronikowska, T. Bronikowski, M. Ulejczyk, Environ. Sci. Technol. 26 (1992) 1976–1981.
[43] W. Yue, Basis of Applied Catalysis, Chemical Industry Press, Beijing, 2009.